# Aerodynamic characteristics of two side-by-side circular cylinders and application of wavelet analysis on the switching phenomenon

Md. Mahbub Alam, M. Moriya, H. Sakamoto*

*Department of Mechanical Engineering, Kitami Institute of Technology, 165 Koen-cho, Kitami, Hokkaido 090-8507, Japan*

## Abstract

The aerodynamic characteristics of two stationary cylinders, both circular and square, in a side-by-side arrangement were investigated experimentally in a uniform flow at a Reynolds number of $5.5 \times 10^4$, although the square cylinder results are rather limited. This Reynolds number is within the range in which fluid forces acting on a single cylinder are comparatively insensitive to change in the Reynolds number. The focus of this study was on the determination of the characteristics of steady and fluctuating fluid forces, wake frequencies and switching phenomena in two side-by-side cylinders. For a spacing ratio of $T/D < 1.2$ ($T$, gap spacing between cylinders; $D$, diameter), the gap flow was biased to one side, resulting in the formation of a narrower wake behind one cylinder and a wider wake behind the other. Steady and fluctuating fluid forces acting on the cylinders were decomposed for the narrower wake and the wider wake flow patterns. For $T/D > 0.20$, the action of lift forces on both cylinders was in an outward direction (repulsive); however, for $T/D = 0.10$, the action of lift force on the cylinder associated with the narrower wake was inward and that on the other cylinder was outward. In the bistable flow regime, $T/D = 0.2-1.2$, when the gap flow switched spontaneously from one side to the other, another short duration stable flow pattern (which can be termed an intermediate flow pattern) persisted in the intermediate time, in which the gap flow was oriented parallel to the free-stream flow and the Strouhal number was almost equal to that of a single cylinder. Flow visualization images and results of modal analysis and wavelet analysis of velocity signals obtained from two hot-wires corroborated the appearance of the intermediate flow pattern. In the case of synchronized vortex shedding and even in the intermediate flow pattern, a predominant antiphase synchronized vortex was found in both the case of two side-by-side circular cylinders and the case of two side-by-side square cylinders.

© 2003 Elsevier Ltd. All rights reserved.

## 1. Introduction

Determination of the characteristics of fluid flow and vortex dynamics around simple configurations of bodies is helpful for understanding the flow around more complex and larger-scale structures. A circular cylinder is one of the elementary shapes of structures or structural components used in engineering practice, and several circular cylinders are often used in groups. Many interesting and unexpected fluid phenomena may occur when two bodies are placed one beside the other (Spivack, 1946; Zdravkovich, 1977; Williamson, 1985), and the grouping effect of bodies is a very interesting subject of fundamental research in fluid mechanics. Two circular cylinders of equal diameters arranged side-by-side is a simple case of such a group (Fig. 1). It is noted that, in Fig. 1, the spacing between the cylinders is denoted

___

*Corresponding author. Tel./fax: +81-157-26-9207.

*E-mail address:* sakamoto@mech.kitami-it.ac.jp (H. Sakamoto).
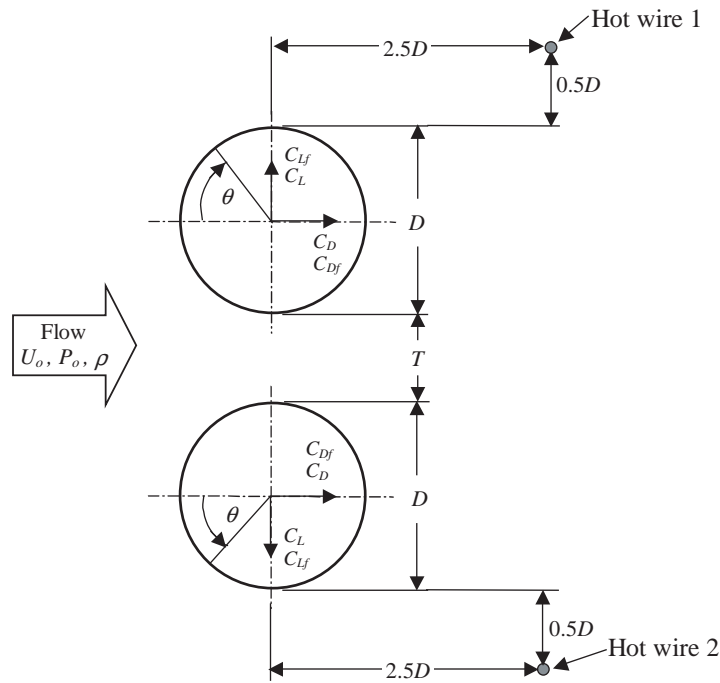
Fig. 1. Sketch of the coordinate system and hot-wire positions.

by $T$, which is the width of the gap between the cylinders, as opposed to center-to-center spacing adopted by other researchers. Many studies have been directed toward the case of a steady flow past two circular cylinders in a side-by-side arrangement (Landweber, 1942; Spivack, 1946; Bearman and Wadcock, 1973; Kamemoto, 1976; Williamson, 1985; Jendrzejczyk and Chen, 1986; Kim and Durbin, 1988; Guillaume and LaRue, 1999; Sumner et al., 1999; Zhang and Zhou, 2001; Zhou et al., 2002).

As the spacing between two side-by-side circular cylinders is varied, two major flow regimes, characterized by the behavior of the wake region, are observed. In the first regime, in which the wake behind the cylinders is grossly unsteady and asymmetric, the gap flow is biased toward one side or the other, and the cylinder toward which the flow is biased consequently has a narrower near wake and higher-frequency vortex shedding (defined as mode 'NW' in the present study), see Fig. 2, while the other cylinder has a wider near wake and lower-frequency vortex shedding (defined as mode 'WW'). Mode 'NW' (narrow wake) causes a higher drag, and the mode 'WW' (wide wake) causes a lower drag on the respective cylinders (Bearman and Wadcock, 1973; Quadflieg, 1977). The biased gap flow is bistable and switches from one side to the other at irregular intervals of time. This regime is therefore known as a flip-flopping regime or bistable flow regime (Bearman and Wadcock, 1973; Zdravkovich, 1977; Kim and Durbin, 1988). The second regime is one in which the wake behind one cylinder is similar to that of the other, and the two wakes exhibit the same frequencies. In this regime of flow, the wakes of the cylinders are either antiphase or in-phase modes (Thomas and Kraus, 1964; Zhou et al., 2001). The vortex patterns associated with these modes are illustrated in Fig. 3. Most investigators have concluded that in-phase and antiphase synchronizations are possible, but a predominance of antiphase shedding was observed by Bearman and Wadcock (1973), Kamemoto (1976), Williamson (1985), Peschard and Gal (1996), Kolar et al. (1997), Sumner et al. (1999), Meneghini et al. (2001), and Zhou et al. (2002). Zhou et al. recently used a phase-averaging technique to elucidate the characteristics and evolution of far-wake vortices during their convection downstream. They found that, for $T/D = 2.0$, vortices that shed from the cylinders form two vortex streets (four rows of vortices), yielding a flow with an antiphase mode which persists until about $30D$ downstream. Liu et al. (2001) simulated flow around two side-by-side cylinders at Re = 200 for $T/D = 2.0$, and they found only in-phase vortex-shedding in their simulation results. However, they observed both in-phase and antiphase vortex shedding in their experimental visualization. It can also be noted that, when an array of two side-by-side cylinders is placed behind two other side-by-side cylinders with equal spacing (a square array of four cylinders), an in-phase pattern of vortices was found to be shed at $T/D = 2.0$ and an antiphase pattern was found to be shed at $T/D = 4.0$ (Farrant et al., 2000).
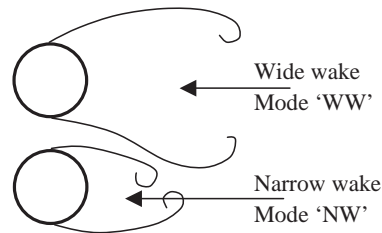
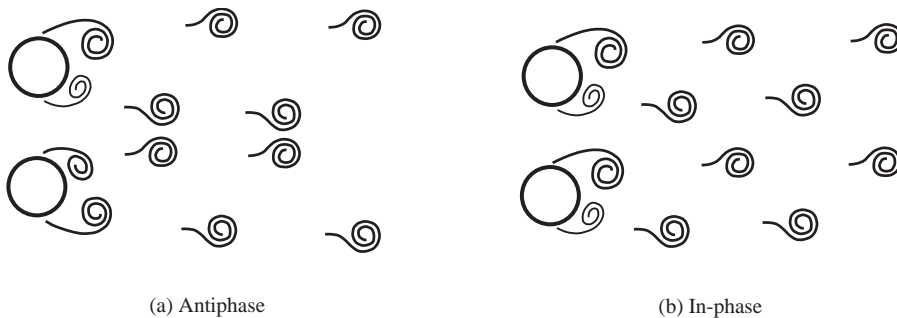Fig. 2. Schematic illustration of an asymmetric wake structure.



(a) Antiphase  (b) In-phase

Fig. 3. Configurations of vortices for two cylinders at a large spacing.

In the bistable flow regime, as mode 'NW' randomly switches to mode 'WW' and vice versa, it is difficult to measure the fluid forces induced by mode 'NW' and mode 'WW' separately. Zdravkovich and Pridden (1977) measured the drag and lift forces for mode 'NW' and mode 'WW' separately. In order to make mode 'NW' and mode 'WW' sufficiently stable, they slightly staggered the cylinders. They found that the sum of low and high drag in the bistable flow regime was always less than twice the drag of a single cylinder. However, Zhou et al. (2001) found that the mean drag of two cylinders was appreciably higher than that of a single cylinder at $T/D = 2.0$. Results obtained by Hori (1959) showed that the sum of the drag of the cylinder pair was greater than that of the two cylinders in isolation for $T/D = 0.2$ and 2.0. The results obtained by Hori agree with those obtained by Zhou et al., but they disagree with those obtained by Zdravkovich and Pridden (1977). The data obtained in previous studies on steady fluid force are inconsistent, and there have been few studies pertaining to unsteady fluid forces acting on two cylinders.

The frequency of vortex shedding behind two side-by-side cylinders in the bistable flow regime is still obscure and discrepant. Results obtained by Bearman and Wadcock (1973) showed that low and high frequencies associated with modes 'WW' and 'NW' were smaller and greater than that of a single cylinder, respectively. Spivack (1946) measured the velocity-fluctuating frequency using a hot-wire probe at a large number of points in the cylinder pair wake, and he found that the vortex shedding frequency for $T/D < 0.30$ was close to that associated with a solid body with the dimensions of the cylinder pair. He also found a second harmonic frequency in certain positions in the flow. Based on the results of flow visualization at a low Reynolds number, Williamson (1985) proposed that the high frequency resulted from the existence of a third harmonic vortex shedding mode and that there also existed a second harmonic frequency mode. He also noted that the frequency of gap flow vortices that are shed as pairs was the same as the frequency of outer vortices of mode 'NW'. On the contrary, Zhou et al. (2001) proposed that the high frequency (in the narrow wake), which is about three times larger than the low frequency is due to squeezing of the pair of vortices from the gap flow to the dominant outer vortices of mode 'NW'.

The aims of the present study were to determine the wake characteristics, switching phenomena and characteristics of aerodynamic forces acting on two circular cylinders placed in side-by-side arrangement and to elucidate the discrepant points. In the present study, fluid forces were separated for modes 'WW' and 'NW' in the bistable flow regime. The frequency of vortex shedding and the switching phenomenon in the bistable flow regime were investigated by wavelet analysis and modal analysis. Measurements were carried out systematically in the range of spacings $T/D = 0.1 - 5$. The results are discussed on the basis of surface pressure distribution, vortex shedding frequency, and visualized flow pattern.

## 2. Experimental details

### 2.1. Wind tunnel

Experiments were conducted in a closed-circuit wind tunnel with a test-section of $300 \times 1200$ mm. The cylinders used as test models were made of brass and were each 49 mm in diameter. The cylinders spanned the horizontal 300 mm dimension of the tunnel. The free-stream velocity, $U_o$, in the tunnel was 17 m/s, giving a Reynolds number (Re) of $5.5 \times 10^4$, based on a single cylinder. Within the middle $240 \times 950$ mm of the test-section, the flow was uniform within $\pm 2\%$ of the centerline velocity. Within the same region, the turbulence intensity was less than 0.5% of the free-stream velocity. A fine-mesh honeycomb that was placed at the entrance of the test-section to provide a uniform flow was responsible for such a high turbulence. In order to check the spanwise uniformity of flow as well as spanwise separation of flow over a single cylinder for fluid forces being measured by a load cell (which will be discussed in the next section), circumferential time-averaged and fluctuating pressures on the surface of the cylinder at the mid-section, and at $\pm 35$ mm and $\pm 80$ mm (from the mid-section), were measured. The results showed that the time-averaged and fluctuating pressure distributions at the five different sections were the same within the accuracy of measurement. The geometric blockage ratio and aspect ratio at the test section were 4 and 6%, respectively. Excluding boundary layer thickness, however, the effective aspect ratio was considered as 5. None of the results presented were corrected for the effects of wind-tunnel blockage.

### 2.2. Fluid force and pressure measurements

Fluid forces acting on the cylinders were measured by a direct measurement method. As shown in Fig. 4(a), the cylinder for the measurements of fluid forces was composed of two parts, an active cylinder and a dummy cylinder; a load cell, on which four semiconductor strain gages were installed to measure fluid forces, was set inside each cylinder. The load cell installed inside the active cylinder measured a combination of fluid forces and forces due to vibration transmitted from the outside through the cylinder support. The load cell installed inside the dummy cylinder measured forces due to vibration transmitted from the outside through the cylinder support. Hence, the fluid forces acting on the active cylinder could be calculated by subtracting the output of the load cell installed inside the dummy cylinder from that installed inside the active cylinder. The load cell had a high linearity in the load/output relation. The sensitivity of the load cells was 11.311 mV/g. The natural frequency of the load cell set in the active cylinder was about 1009 Hz, whereas the measured frequency of the fluctuating lift ranged from approximately 20–140 Hz. Thus the natural frequency of the load cell was 7.2–50 times greater than the frequency of fluctuating lifts. According to So and Savkar (1981), a natural frequency of at least four times that of the dominant force frequency is required for the measurement system to work with reasonable accuracy. Therefore it is considered that the fluctuating fluid forces could be measured without introducing a resonant problem. The spanwise size of the active cylinder was 45 mm (0.92 times the diameter of the cylinder). This size was determined by taking into account the cross-correlation length of fluctuating pressure in the spanwise direction of the cylinder. The details of the load cells and fluid force measurement procedure have been described by Sakamoto and Oiwake (1984) and Sakamoto et al. (1994). The force measurement was carried out to measure the local fluid forces over the small span (45 mm) of the cylinder and the small span (load cell) was located at the middle of the spanwise length of the cylinder as well as the middle of the wind tunnel.

A semiconductor pressure transducer (Toyoda PD104K) located at the mid-section of the cylinder was used to measure the surface pressure during the experiments, and the transducer output was calibrated to give a reading of 6.22 V for 1 kPa of applied pressure. The pressure transducer was set just below the surface of the model and communicated to the surface through a pressure connection of size 0.8 mm diameter by 1.5 mm long, as shown in Fig. 4(b). The dynamic response characteristics of the transducer were in the range of frequency 0–550 Hz. The transducer responded reasonably to the pressure fluctuations up to 500 Hz with a gain factor of $1 \pm 0.06$, the phase lag being negligible. This frequency was well above the frequency of vortex shedding from the cylinders.

### 2.3. Flow visualization

Flow visualization was carried out in a water channel with a $250 \times 350$ mm working section and 1.5 m long. A fine-mesh honeycomb was used to remove any large-scale irregularities. In the flow visualization test, two circular tubes with identical diameter of 20 mm were used. The flow visualizations in water were conducted at a Reynolds number of 350. This Reynolds number is beyond the transition range to turbulence in the wake. Fully turbulent shedding conditions prevail for Re > 300 (Williamson, 1996). The flow was visualized by using the hydrogen bubble technique, involving a platinum wire of 0.02 mm in diameter.
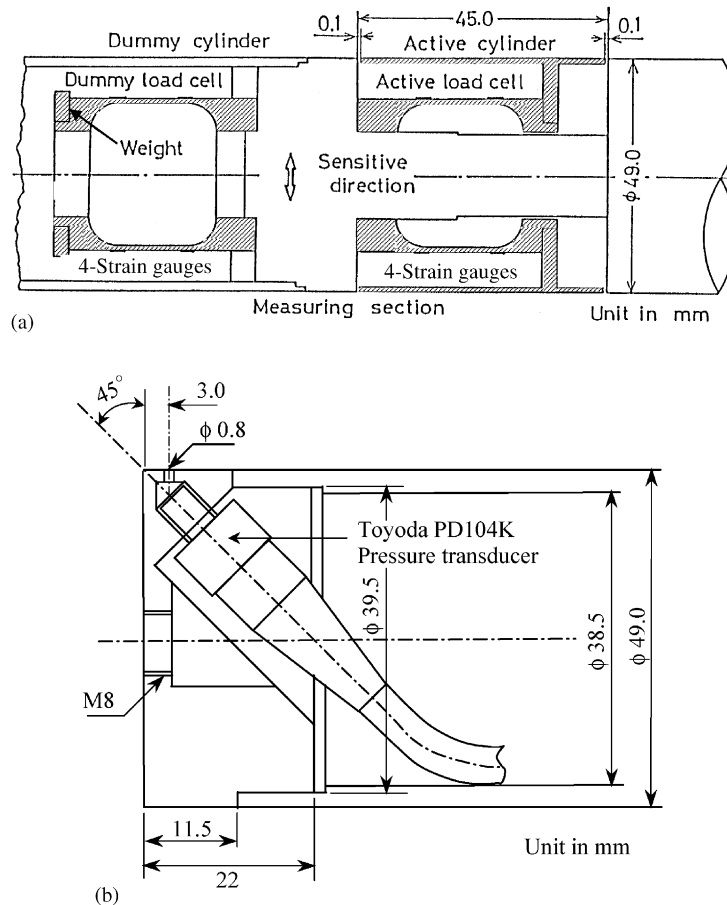
Fig. 4. Installation of: (a) load cells inside a cylinder, (b) pressure transducer inside a cylinder.

## 2.4. Vortex shedding frequency measurement

Two single hot-wire probes with diameter of 4 mm were used to measure vortex shedding frequencies behind the cylinders. The hot-wires were positioned $1D$ outside and $2.5D$ downstream from the centers of the cylinders (Fig. 1). The hot-wire signals were digitized with sampling frequency of 3.6 kHz, corresponding to about 28 and 120 samples/period for maximum and minimum frequencies detected during experiment. Fourier power spectra of hot-wire signals were based on the average of five runs, each run composed of 1024 samples.

## 2.5. Signal processing

We found two major patterns of force signals in the bistable flow regime, $T/D = 0.1-1.5$. These two patterns are due to modes 'NW' and 'WW' as described in the Introduction. Accordingly, in the bistable flow regime where fluid forces switch randomly, it is necessary to separate the fluid force coefficients [such as $C_L$ (lift coefficient), $C_{Lf}$ (fluctuating lift coefficient), $C_D$ (drag coefficient), $C_{Df}$ (fluctuating drag coefficient), $C_P$ (pressure coefficient), and $C_{Pf}$ (fluctuating pressure coefficient)] for the modes 'NW' and 'WW'. During the experiment, the gap flow switched spontaneously from one side to the other.

Next, we will discuss the sequential steps for evaluating the fluid force coefficients separately for modes 'NW' and 'WW'. As an example, the signal of instantaneous lift, $C_{Li}$, as shown in Fig. 5(a), possesses two patterns of signals, with some portions having low $C_L$ (due to the 'NW' mode) and some having high $C_L$ (due to the 'WW' mode). First, as defined in Eq. (1), the local average $C_{Lp}$ of $C_{Li}$ was calculated for the time interval corresponding to digitized $N$ data
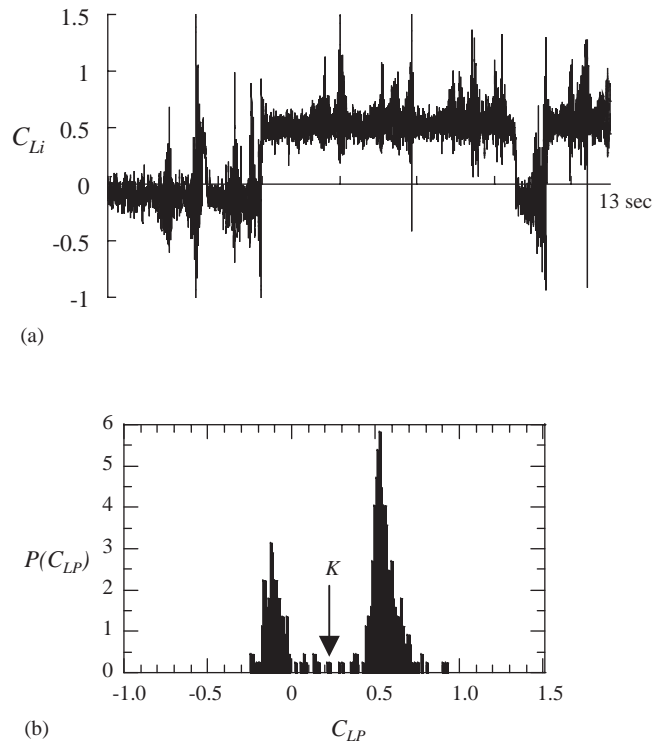
Fig. 5. (a) Input signal ($T/D = 0.10$) and (b) probability density distribution of local average, $C_{LP}$, of signal (a).

counted from a peak to the $i$th (the next peak) data,

$$C_{Lp}(i, N) = \frac{1}{N} \sum_{j=i+1}^{i+N} C_{Li}(j). \tag{1}$$

To obtain the peaks with reasonable accuracy, high-frequency noises were eliminated from digitally stored data by using a low-pass filter, while the original data were stored. Then a probability density distribution, $P(C_{Lp})$, of the values of $C_{Lp}$ was constructed to find a frequency-bound value that separates $C_L$ for modes 'NW' and 'WW', as shown in Fig. 5(b). It is clear from the figure that the values of $C_{Lp}$ are closely arranged around two values of $C_{Lp}$ ($C_{Lp} = -0.15$ and 0.55). The appearance of two peaks implies that the input signal is composed of two major patterns whose individual averages are near $-0.15$ and 0.55. Thus the value of $C_{Lp}$ denoted by $K$ can be assumed to be the frequency boundary between the 'NW' and 'WW' modes. By determining the value $K$, the prerecorded input signal in the form of digital data into the memory is portioned out into modes 'NW' and 'WW' for $C_{Lp} < K$ and for $C_{Lp} \geqslant K$, respectively. Then the average and r.m.s. values of the data for mode 'NW' were calculated to obtain the lift coefficient, $C_L$, and the fluctuating lift coefficient, $C_{Lf}$. Similarly, $C_L$ and $C_{Lf}$ for mode 'WW' were calculated. As there were two values of $C_D$ for the two different flow patterns, $C_D$ and $C_{Df}$ for modes 'NW' and 'WW' were divided in the same way as described above. The overall uncertainties in $C_D$, $C_{Df}$ and $C_{Lf}$ were estimated to be $\pm 2\%$, $\pm 4\%$ and $\pm 3.5\%$, respectively.

## 3. Results and discussion

### 3.1. Effect of blockage and aspect ratio on fluid forces

In our experiment, the blockage ratio was 4% for a single cylinder; however, total blockage for the cylinder pair was 8%. As discussed by West and Apelt (1982), the effect of blockage on time-averaged drag was unaffected by blockage for blockage ratios less than 6% and there is a very small difference in blockage effect between the blockage ratio of 6% and 8%. So, the blockage effect in the present results is expected to be small. The effect of aspect ratio on the fluctuating

Table 1
Comparison of fluid force coefficients

| Author | Reynolds number | Blockage ratio (%) | Aspect ratio | Turbulent intensity | $C_D$ | $C_{Df}$ | $C_{Lf}$ |
|---|---|---|---|---|---|---|---|
| Keefe (1961) | $5.2 \times 10^4$ | 4 | 18 | Low | — | — | 0.47 |
| Bearman (1969) | $2 \times 10^5$ | 6.5 | 12 | 0.2% | 1.14 | — | — |
| Lesage and Gartshore (1987) | $6.5 \times 10^4$ | 4.1 | 18 | — | 1.19 | — | 0.45 |
| Szepessy and Bearman (1992) | $5.1 \times 10^4$ | 7.7 | 6.5 | 0.05% | — | — | 0.49 |
|  | $4.3 \times 10^4$ | 7.7 | 5 | 0.05% | — | 0.15 | — |
| Nebres and Batill (1993) | $3 \times 10^4$ | 7.3 | 10.3 | 0.06% | 1.12 | — | — |
| West and Apelt (1997) | $5.6 \times 10^4$ | 9.5 | 15 | 0.2% | — | 0.13 | 0.47 |
| Present | $5.5 \times 10^4$ | 4 | 6 | 0.5% | 1.12 | 0.14 | 0.48 |

fluid forces at different ranges of Reynolds numbers is different and the fluctuating fluid forces are dependent also on turbulence intensity and blockage ratio (Szepessy and Bearman, 1992; West and Apelt, 1997). West and Apelt (1993) established that the fluctuating fluid forces on an elemental section are independent of spanwise location for aspect ratios greater than 10, i.e., 'long' cylinder conditions occur. From the result published by Szepessy and Bearman (1992), it was found that the fluctuating lift force was about 3% and 5% higher for an aspect ratio of 6 and 5, respectively, than that for the aspect ratio of 10. A comparison of $C_D$, $C_{Df}$, and $C_{Lf}$ for a single cylinder obtained in the present study with those obtained by others is presented in Table 1. It can be noted that Keefe (1961) measured $C_{Lf}$ using strain gages connected to a spanwise length of $1D$, and the data from West and Apelt (1997) were also for a spanwise length of $1D$ and were obtained from an integration of the cross-correlation curve. The values of $C_{Lf}$ and $C_{Df}$, measured for a spanwise length of $0.92D$ in the present case, agree well with those obtained by other researchers mentioned in Table 1. By integrating the time-averaged pressure around a single cylinder, $C_D$ was evaluated to be 1.15 which is comparable to the value of 1.12 obtained from the direct measurement method.

### 3.2. Steady fluid forces

Fig. 6 shows the drag coefficient, $C_D$, distribution for two cylinders in a side-by-side arrangement. The results obtained by Zdravkovich and Pridden (1977) and Hori (1959) are also included in the same figure for comparison. Unfortunately, their data are too sparse to show the actual trend of $C_D$ variation. Two values of $C_D$ for two different flow patterns (modes 'NW' and 'WW') on a cylinder were decomposed as shown in the figure. The process of the decomposition of $C_D$ for modes 'WW' and 'NW' has been discussed in Section 2.5. For $T/D > 1.5$, the gap flow was not biased and both cylinders experienced the same drag behavior. The value of $C_D$ for $T/D > 3$ is almost equal to that of a single cylinder, i.e., there is virtually no interference effect between the cylinders.

In the bistable flow regime, $T/D = 0.10 - 1.50$, the difference between the magnitudes of $C_D$ for modes 'NW' and 'WW' is larger for small spacings. The magnitude of $C_D$ at $T/D = 0.10$ for mode 'NW' is 1.69 which is 1.5 times greater than that of a single cylinder. Liu et al. (2001) and Slaouti and Stansby (1992) also found such a high $C_D$ in their simulation results for $T/D = 0.10$ at a low Reynolds number. They found the same magnitude of $C_D$ on both cylinders. Liu et al. evaluated $C_D$ as 1.80 and Slaouti and Stansby evaluated $C_D$ as 1.85 for $T/D = 0.10$. The existence of two values of $C_D$ on the cylinders, as seen in Fig. 6, is logical since there is a biased gap flow. It should be pointed out that Zdravkovich and Pridden (1977) noted that the mean value of $C_D$ of the two cylinders (modes 'NW' and 'WW') is always less than that of a single cylinder. In the range of $T/D = 0.10 - 0.20$ and 1.20–1.50, we found that the mean $C_D$ value of the cylinders is greater than that of a single cylinder. The data obtained by Hori (1959) show that the mean $C_D$ of two cylinders is greater than that of a single cylinder for $T/D = 0.2$ and 2.0. Note that the value $C_D$ of a single cylinder for the case of Hori was 1.09. Thus, the present results agree well with those obtained by Hori.

It is almost intuitive that, the wider the wake, the higher the drag. In the case of two side-by-side cylinders, however, the lower and the higher drag values are accompanied by the wider (mode 'WW') and the narrower (mode 'NW') wakes, respectively, which is exactly opposite to intuition. The higher drag accompanied by mode 'NW' in two side-by-side cylinders is mainly due to a nearer rolling position of the shear layers and due to higher wake velocities mostly contributed from the gap flow. This can clearly be understood from a note by Roshko (1954); he noted, "Generally, for a given cylinder a decrease in wake width corresponds to an increase in drag, which seems at variance with intuition. However, the decrease in width is associated with an increase in 'wake velocities,' the net effect being an increased wake energy corresponding to the increased drag."
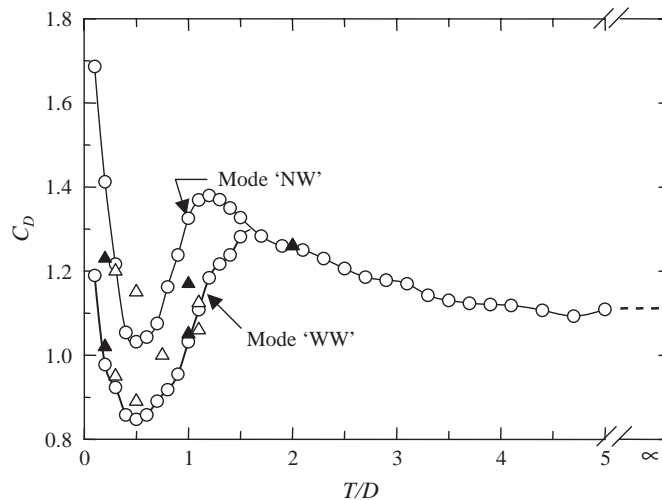
Fig. 6. Drag coefficient, $C_D$, distribution: ○, present; △, Zdravkovich and Pridden (1977), Re $= 6 \times 10^4$; ▲, Hori (1959), Re $= 8 \times 10^3$; - - -, single cylinder (present).



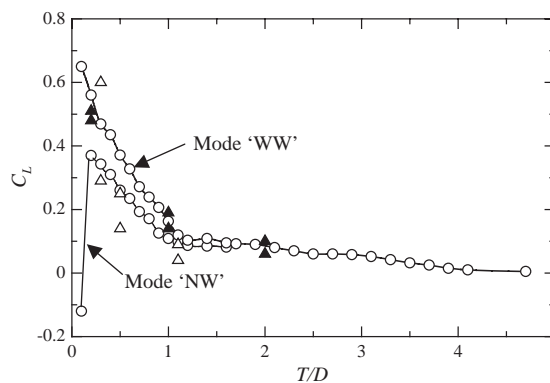Fig. 7. Lift coefficient, $C_L$, distribution: ○, present; △, Zdravkovich and Pridden (1977), Re $= 6 \times 10^4$; ▲, Hori (1959), Re $= 8 \times 10^3$.

The variation in lift coefficient, $C_L$, as a function of spacing ratio is shown in Fig. 7. In this study, a repulsive (outward direction) force was considered as positive, and an attractive (inward direction) force was considered as negative. For the range of $T/D = 0.5$–$1.5$ where the difference in $C_L$ between the two modes is small, the lift force signal of a cylinder and the base pressure ($\theta = 180°$) signal of the other cylinder were stored simultaneously, and the base pressure signal was used a reference signal to differentiate the data of $C_L$ for modes 'NW' and 'WW'. The lift force coefficient at $T/D = 0.10$ is interesting. The coefficients are $-0.12$ and $0.65$ for modes 'NW' and 'WW', respectively; i.e., there is a large difference between the values, and attractive force is also possible for two side-by-side cylinders in the bistable flow regime. In previous investigations by Hori (1959), Jendrzejczyk and Chen (1982), Zdravkovich and Pridden (1977), and Bearman and Wadcock (1973), it was noted that lift force acting on the cylinders was always repulsive.

In order to determine the nature of the flow pattern that induced negative lift force on the cylinder, the pressure coefficient, $C_P$, was also evaluated separately for modes 'NW' and 'WW' at $T/D = 0.10$, and the results are shown in Fig. 8. In this case, the lift force signal of a cylinder and the pressure signal of the other cylinder were stored simultaneously so that the lift force signal could be used as a reference signal to identify $C_P$ for modes 'NW' and 'WW'. It can be seen in the figure that the stagnation point (positive pressure region) shifts toward the inner side at $330°$ instead of $0°$, and this is a cause of repulsive lift force. In the case of mode 'NW', there is a big difference between the pressure at the inside surface and the outside surface. The pressure at the inside surface is more negative than that at the
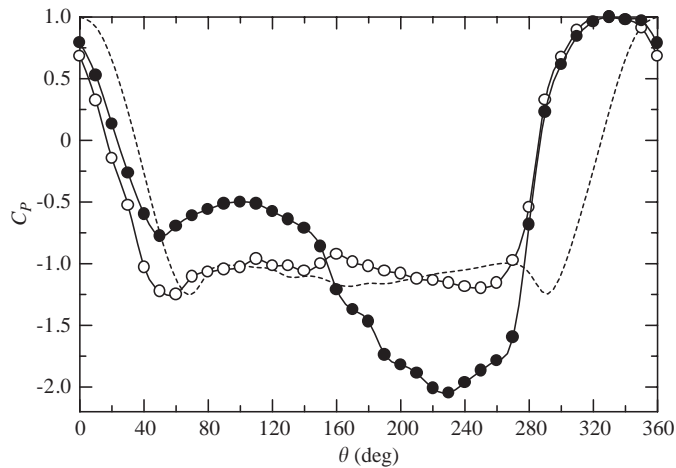
Fig. 8. Pressure coefficient, $C_P$, distributions for $T/D = 0.10$: $\bigcirc$, mode 'WW'; $\bullet$, mode 'NW'; - - - -, single cylinder.

outside surface; thus, the difference between pressures at the outside and inside surfaces is directed toward the inside. This pressure difference dominates the component of lift force that is due to the shift of the positive pressure region (stagnation point); consequently, the resultant lift force is directed inward (negative $C_L$). The values of $C_D$ and $C_L$ determined from integrating the surface pressure presented in the figure were 1.72 and $-0.14$, respectively, for mode 'NW', and 1.21 and 0.61, respectively, for mode 'WW'. Thus the pressure distribution corroborates the negative lift. The pressure distributions indicate that the outer shear layer can be expected to separate from the cylinder at $\theta = 60°$ and $65°$ for modes 'WW' and 'NW', respectively, while gap flow separation can be expected at about $\theta = 240°$ and $200°$ for modes 'WW' and 'NW', respectively.

The flow visualization pattern and corresponding sketch shown in Fig. 9 give a clear conception about the flow pattern discussed above. The flow pattern shows that an earlier separation of the gap flow occurs from the lower cylinder (positive $C_L$) and that the gap flow is directed along the surface of the upper cylinder, and finally the gap flow separates near the base of the cylinder. The lift force acting on the cylinders can also be explained in terms of circulation, which is defined as the line integral about a closed path (periphery of the cylinder) of the tangential velocity component along the path. It is obvious from the figure that the net circulation around the lower cylinder is certainly anticlockwise, thus producing a downward (positive) lift force. On the other hand, as the gap flow is directed along the periphery of the upper cylinder for a longer peripheral length, the net circulation around the cylinder is counterclockwise, resulting in a downward (negative) lift force on the upper cylinder. It is evident that the lift force acting on the cylinders associated with mode 'NW' depends on the deflection (bias) of the gap flow. Sumner et al. (1999) estimated the gap flow deflection angle from flow visualization images and PIV results. The deflection angle is the angle between the gap flow direction and direction of the free-stream flow. Their data showed a large difference between the deflection angles at $T/D = 0.125$ and 0.25. Hence, a large difference in $C_L$ in the mode 'NW' at $T/D = 0.1$ and 0.2 (Fig. 7) is possible. In both a wind-tunnel test (Re $= 5.5 \times 10^4$) and flow visualization test (Re $= 350$), it was found that, at $T/D = 0.10$, the outer shear layers shed alternately ($180°$ phase difference) and the gap flow shed in-phase ($0°$ phase difference) with the outer shear layer of mode 'WW'; in other words, the adjacent shear layers of the cylinder, toward which the gap flow is biased, shed alternately, as is seen in the photographs. Direct correspondence between the Reynolds numbers 350 (water channel experiment) and $5.5 \times 10^4$ (wind tunnel experiment) is only qualitative. However, a compilation of previous studies [Kamemoto (1976), Re $= 662$ and $3 \times 10^4$; Kiya et al. (1980), Re $= 1.58 \times 10^4$; Williamson (1985), Re $= 50$–200; Kim and Durbin (1988), Re $= 2.2 \times 10^3$–$6.2 \times 10^3$; Mizushima and Takemoto (1996), Re $= 80$–320; Peschard and Gal (1996), Re $= 90$–150; Zhou et al. (2002), Re $= 5.8 \times 10^3$] showed that there was no basic phenomenological difference (particularly the behavior of switching flow) in the results of two side-by-side cylinders at various Reynolds numbers. So a qualitative comparison can be done between the results obtained at Re $= 350$ and $5.5 \times 10^4$.

The pressure distribution for $T/D = 0.50$, at which $C_D$ for both modes is minimum, shown in Fig. 10. The trends in variation of $C_P$ for modes 'NW' and 'WW' are almost the same except for a difference in pressures in the base region. At this spacing, the stagnation point is at $\theta = 340°$. Similarly, the stagnation points were at $\theta = 350°$, $355°$ and $360°$ ($0°$) for $T/D = 0.90$, 1.40, and 3.0, respectively.
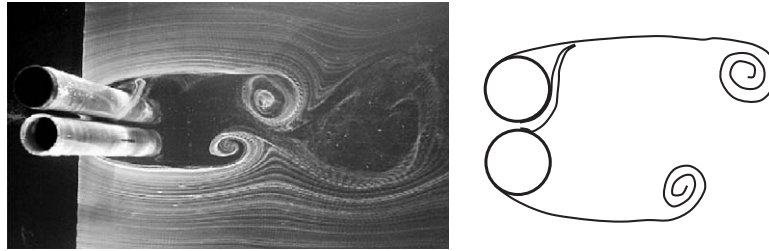
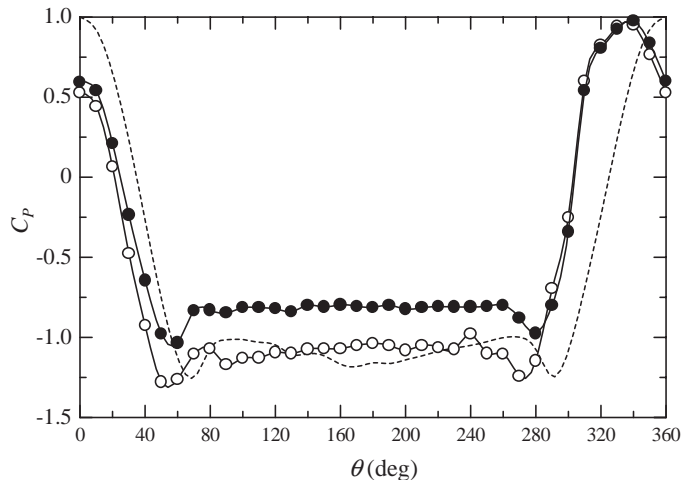Fig. 9. Visualized flow pattern and corresponding sketch ($T/D = 0.10$).



Fig. 10. Pressure coefficient, $C_P$, distributions for $T/D = 0.50$: ○, mode 'NW'; ●, mode 'WW'; ----, single cylinder.

### 3.3. Fluctuating fluid forces

Fluctuating drag-coefficient, $C_{Df}$, and fluctuating lift-coefficient, $C_{Lf}$, distributions for two cylinders are shown in Fig. 11. It can be seen that the fluctuating drag and lift values are very small at and near $T/D = 0.50$. Jendrzejczyk and Chen (1982, 1986) also measured $C_{Df}$ and $C_{Lf}$ for $T/D = 0.35$ and 0.5 and noted that $C_{Df}$ and $C_{Lf}$ were not affected by the biased flow pattern; there was a very small difference between the fluctuating force coefficients of the two cylinders. At $T/D = 0.50$, they obtained values of $C_{Df}$ of 0.03 (cylinder 1) and 0.04 (cylinder 2) and values of $C_{Lf}$ of 0.05 (cylinder 1) and 0.06 (cylinder 2) at a Reynolds number of $5 \times 10^4$, with a turbulence intensity of 2.3%. In the figure, apparently, the difference between values of $C_{Df}$ due to the mode 'NW' and mode 'WW' is comparatively larger in the range of $T/D = 0.80-1.2$. In this range of $T/D$, the difference in $C_{Lf}$ is also large. For $T/D > 3$, $C_{Df}$ and $C_{Lf}$ are identical to those of a single cylinder.

Fig. 12 shows the fluctuating pressure coefficient, $C_{Pf}$, distribution for $T/D = 0.10$. The trends in the $C_{Pf}$ distributions for modes 'NW' and 'WW' are very different. It is known that separation of a shear layer causes a peak in the $C_{Pf}$ distribution very near to the separation point (Batham, 1973; Alam et al., 2003). If so, the separation position of the gap flow can be expected to be at 240° and 200° for modes 'WW' and 'NW', respectively. It can be seen that $C_{Pf}$ caused mainly by the outer shear layer ($\theta = 0-110°$) is weaker in the case of mode 'NW' than in the case of mode 'WW'. In the case of mode 'NW', $C_{Pf}$ is high in the base region as well as on the inside surface. That is, higher values of $C_{Lf}$ and $C_{Df}$ in mode 'NW' than in mode 'WW' are mostly from the pressure fluctuations caused by the gap flow. Fig. 13 shows the $C_{Pf}$ distributions for $T/D = 0.50$ and 1.40, at which the fluctuating fluid force acting on the cylinders is minimum and maximum, respectively. For $T/D = 0.50$, $C_{Pf}$ on the whole surface is quite small in comparison with that of the single cylinder and there is a very small difference in $C_{Pf}$ due to modes 'NW' and 'WW'. For $T/D = 1.40$, $C_{Pf}$ for both modes is larger than that of a single cylinder. It is apparent that the outer shear layers separate at $\theta = 70°$ from both cylinders and that the gap flow separates at 280° and 270° for the cylinders with modes 'WW' and 'NW', respectively.
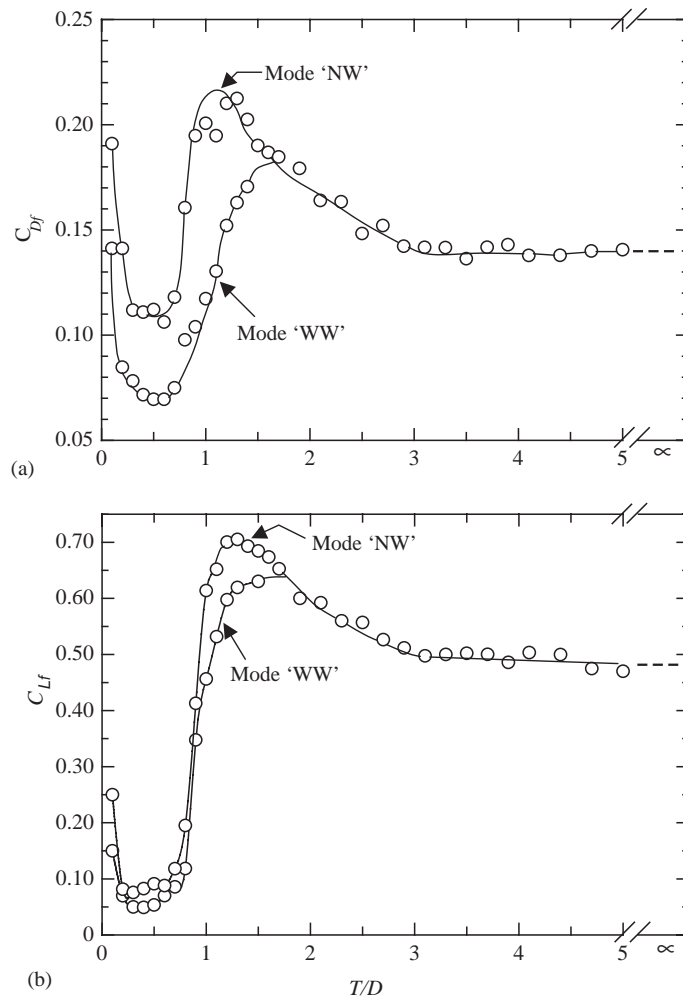
Fig. 11. Fluctuating fluid force coefficient distributions: (a) fluctuating drag coefficient, $C_{Df}$; (b) fluctuating lift coefficient, $C_{Lf}$; ----, single cylinder.

### 3.4. Strouhal number and switching phenomenon

The Strouhal number, St, obtained from the results of Fourier spectral analysis of fluctuating lift force, fluctuating pressure at $\theta = 90°$ and fluctuating velocity obtained by hot-wire probes is shown in Fig. 14 as a function of $T/D$. At a value of $T/D > 1.2$, both Strouhal numbers for the two cylinders are the same as that for a single cylinder. The Strouhal number of a single cylinder was 0.186 in our experiment. The trends of Strouhal number distributions indicated by the high-frequency mode and low-frequency mode agree well with previously published data (Spivack, 1946; Bearman and Wadcock, 1973; Kamemoto, 1976; Kiya et al., 1980; Kim and Durbin, 1988). The high-frequency mode refers to mode 'NW' and the low-frequency mode refers to mode 'WW'. In this study, we found another set of Strouhal numbers whose values lie between the Strouhal numbers associated with the high-frequency mode and those associated with the low-frequency mode. So, we identify the new set of frequencies (Strouhal numbers) as intermediate frequencies. The values of Strouhal numbers associated with the intermediate frequencies are identical to those for $T/D > 1.20$ as well as for a single cylinder. It seems that there is another mode of flow pattern that corresponds to the intermediate Strouhal number. It also seems that, since the Strouhal number associated with the intermediate frequency is the same as that for $T/D > 1.20$, the flow pattern that appears at $T/D > 1.20$ (synchronized flow pattern) continues to appear intermittently in the range of spacing $T/D = 1.10-0.20$. The peak at the intermediate frequency in the power spectrum was less discernible for small spacing; however, as the spacing was increased from $T/D = 0.20$ to 1.20, the peak at the
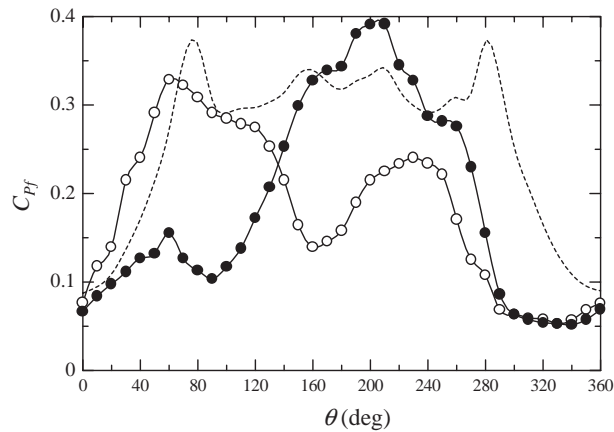
Fig. 12. Fluctuating pressure coefficient, $C_{Pf}$, distributions for $T/D = 0.10$: ○, mode 'WW'; ●, mode 'NW'; - - - -, single cylinder.
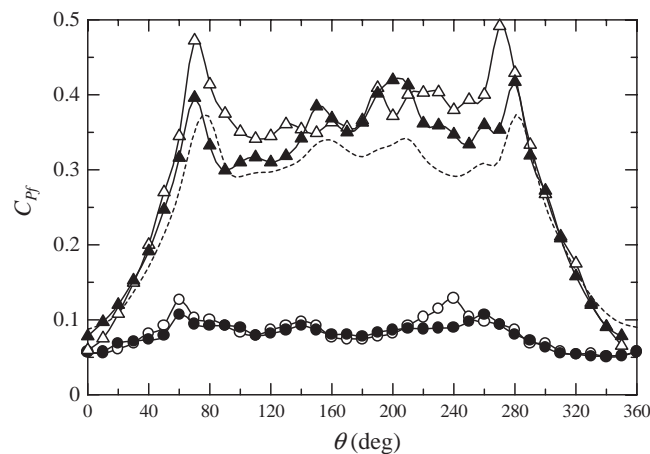


Fig. 13. Fluctuating pressure coefficient, $C_{Pf}$, distributions: ○, mode 'NW', $T/D = 0.50$; ●, mode 'WW', $T/D = 0.50$; △, mode 'NW', $T/D = 1.40$; ▲, mode 'WW', $T/D = 1.40$; - - - -, single cylinder.

intermediate frequency became dominant as seen in Figs. 14(b) and (c). The appearance of the intermediate frequency in the two side-by-side cylinders bears a resemblance to the appearance of a frequency approximately equal to that of a single cylinder in a case of three side-by-side cylinders with unequal spacing (Zhang and Zhou, 2001). For three side-by-side cylinders with $T/D = 0.5D$ and $0.6D$, Zhang and Zhou found that the gap flow passing through the $0.5D$ gap was biased toward the central cylinder and the gap flow passing through the $0.6D$ was no longer biased. As a result, the outer cylinder associated with spacing of $0.6D$ was accompanied by a wake similar to that of a single cylinder and corresponded to a Strouhal number of 0.228. On the other hand, the other outer cylinder and the central cylinder corresponded to Strouhal numbers of 0.076 and 0.518, respectively.

For $T/D = 0.10$, the two cylinders tend to act like a single body and the Strouhal number based on the actual characteristic width is $f(2.1D)/U_o = 0.185$, similar to the Strouhal number of a single cylinder. It has been mentioned that a bistable flow appears in the range of $T/D = 0.10-1.50$; however, Strouhal numbers of the high-frequency mode and the low-frequency mode merge at $T/D = 1.20$ and vortex shedding becomes synchronized for $T/D > 1.20$. Thus, in the range of $T/D = 1.20-1.50$, vortex shedding is synchronized, but the gap flow is slightly biased to one side. The data measured by Bearman and Wadcock (1973) also show that flow is biased for $T/D = 0.10-1.40$; however, vortex shedding is synchronized for $T/D > 1.0$. This implies that synchronization of frequency is possible in the case of asymmetric wakes also.

In order to demonstrate the appearance of the intermediate frequency mode and to elucidate the switching phenomenon, we were interested in the mode analyses. Mode analyses were carried out by using a band-pass filtering
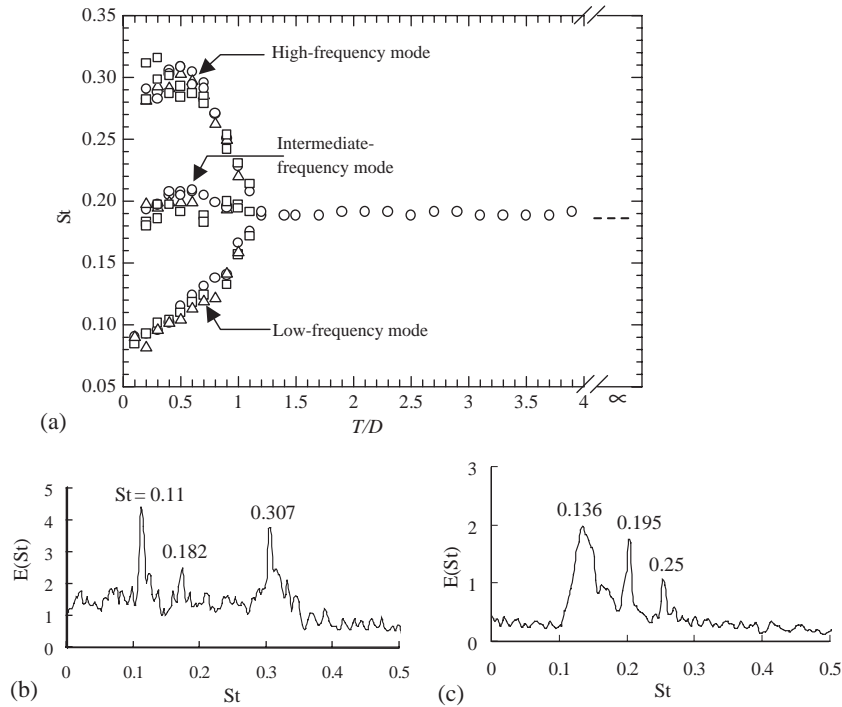
Fig. 14. (a) Strouhal number distribution: $\bigcirc$, fluctuating lift; $\triangle$, fluctuating pressure; $\square$, hot-wire; (b) power spectrum, $T/D = 0.50$; (c) power spectrum, $T/D = 0.90$.
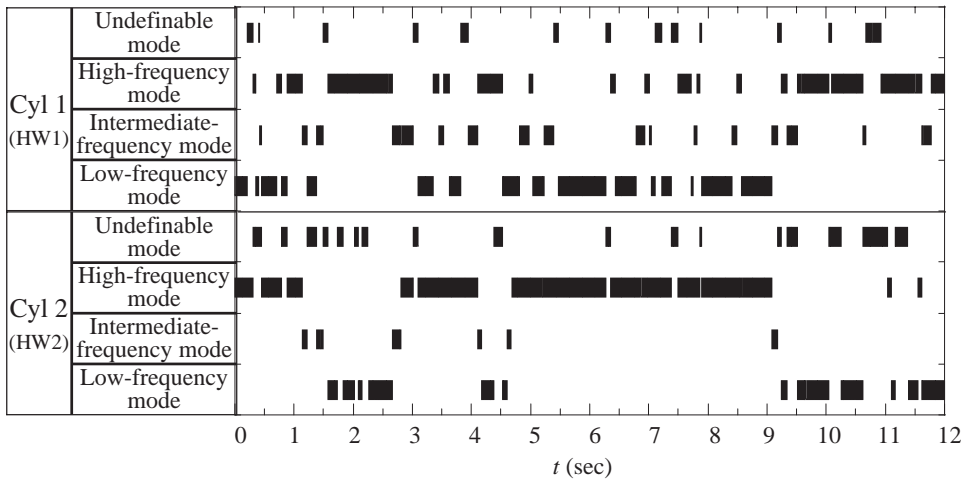


Fig. 15. Timing chart of appearance of various modes for $T/D = 0.70$ (HW1: hot-wire 1; HW2: hot-wire 2).

technique. We chose a spacing of $T/D = 0.70$ at which Strouhal numbers for the high-frequency mode, intermediate-frequency mode and low-frequency mode are approximately 0.125 (43.5 Hz), 0.185 (64 Hz), and 0.28 (97 Hz), respectively; the high and intermediate Strouhal numbers are not harmonics of the low Strouhal number. In some previous investigations, it was found that the higher Strouhal number was a third harmonic of the lower Strouhal number (Williamson, 1985; Mahir and Rockwell, 1996; Zhou et al., 2001).

The signals obtained simultaneously from two hot-wire probes positioned as shown in Fig. 1 were passed through a band-pass filter with band-pass frequencies of 107–92, 72–58 and 48–38 Hz to obtain signals of high frequency,
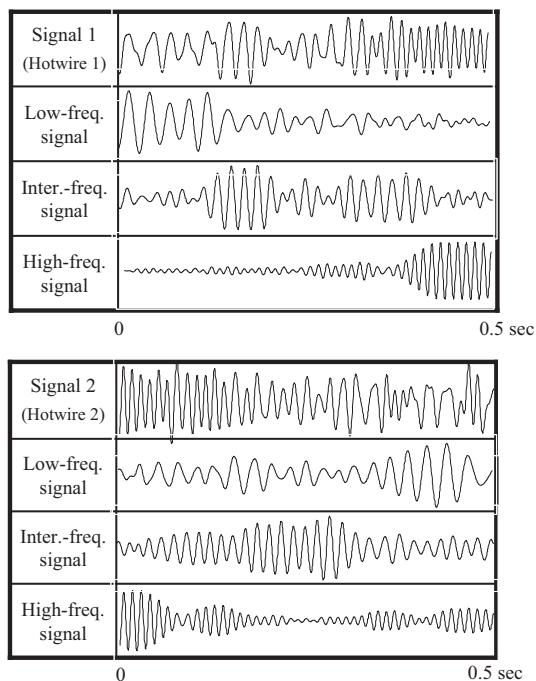
Fig. 16. Decomposition of hot-wire signals by using a digital band-pass filter.

intermediate frequency and low frequency, respectively. Therefore, a set of three signals from hot-wire 1 and another set of three signals from hot-wire 2 were obtained. The local r.m.s. of each filtered signal was calculated, and by comparing the r.m.s. values of three signals of the first set, a mode was chosen for the first cylinder. Similarly, the second mode was chosen from the second set of signals for the second cylinder. Therefore, a timing chart of the appearance of various modes was made, and the results are shown in Fig. 15. Here we have presented another mode, named 'undefinable mode', whose frequency did not fall within these frequencies of modes or whose amplitude of fluctuation was very small. It can be seen in the figure that major switching occurs at time $t = 1.2, 2.8, 4.2, 4.7$, and $9.1$ s. It is interesting that the frequency of a cylinder switches from a low-frequency mode to an intermediate-frequency mode to a high-frequency mode in the case of major switching, while that of the other switches from the high-frequency mode to the intermediate-frequency mode to the low-frequency mode. It can also be seen that sometimes only the low-frequency mode switches to an intermediate-frequency mode or to a high-frequency mode and returns to the low frequency mode. A portion of the signal and its filtered signals that include a switching are presented in Fig. 16 as an example. It can be observed in the figure that, initially, signal 1 is at a low frequency, while signal 2 is at a high frequency, then signals 1 and 2 switch to an intermediate frequency, and finally signals 1 and 2 switch to high and low frequencies, respectively. The flow pattern shown in Fig. 17 gives a clear picture of the switching phenomenon. The gap flow switches as shown in the figure from (a) to (b) to (c). Here pattern (b) with a symmetrical near wake and nonbiased gap flow can be regarded as an intermediate flow pattern that is associated with the intermediate frequency. Since the near wake flow behind each of the cylinders resembles a single cylinder flow, the frequency (intermediate frequency) behind each of the cylinders can be expected to be approximately equal to that of a single cylinder. Similarly, Fig. 18 shows a biased flow pattern and a nonbiased flow pattern at $T/D = 0.70$. It is clear that the nonbiased flow pattern is in the antiphase mode. Even for a small spacing of $T/D = 0.125$, a flow pattern with a symmetrical near wake and nonbiased gap flow was observed in the PIV results obtained by Sumner et al. (1999). They found three kinds of gap flow behavior at $T/D = 0.125$, nonbiased gap flow, biased gap flow, and almost no flow in the gap.

The switching phenomenon and appearance of the intermediate-frequency mode can be studied by wavelet transforms of the hot-wire signals of velocity fluctuation. For a given one-dimensional function $u(t)$, the wavelet transform can be defined as

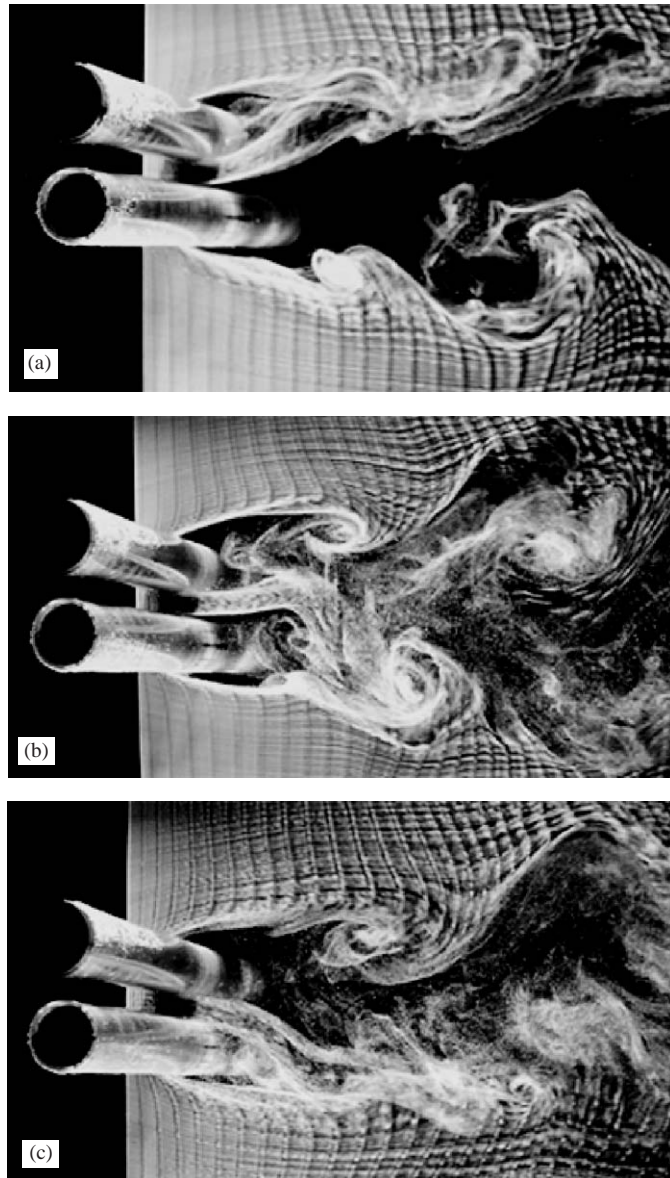$$W(s,b) = p(s) \int u(t) \Psi^* \left( \frac{t-b}{s} \right) \mathrm{d}t, \tag{2}$$

Fig. 17. Visualized flow pattern for the switching phenomenon ($T/D = 0.40$).

where $W(s, b)$ is the wavelet coefficient, the superscript "$*$" denotes the complex conjugate, "$b$" is the translation parameter, "$s$" is the scale parameter, and $p(s)$ is a weighting function that can be chosen as $s^{-1}$, $s^{-1/2}$, $s^{1/2}$, or $s^{0}$ depending on the purpose (Farge, 1992; Lewalle, 1994; Arneodo et al., 1988; Hamdan et al., 1996). In this study, $p(s)$ was chosen as $s^{-1/2}$, so that all wavelets have the same energy at each scale; $\psi(t)$ is a function called the analyzing wavelet or the mother wavelet. A well-known function, such as the Morlet function or the Mexican hat function, is often used as the mother wavelet. The Mexican hat function has a better time resolution property but a poorer frequency resolution property. The Morlet function, however, has a better frequency resolution property. The Morlet and the Mexican hat functions are complex- and real-valued wavelets, respectively. For a real-valued wavelet function, the phase property in the signal is undefined. In the present study, the Morlet function was used as a mother wavelet and is written as

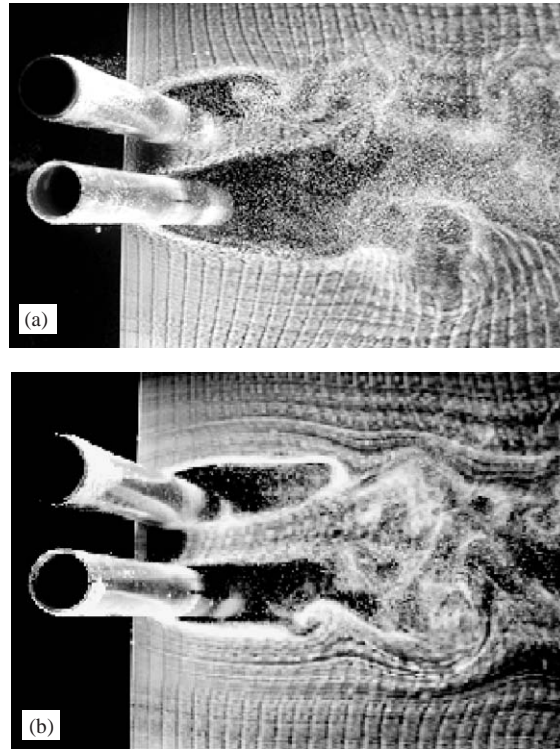$$\Psi(\eta) = e^{i\omega_0\eta}e^{-\eta^2/2}, \tag{3}$$

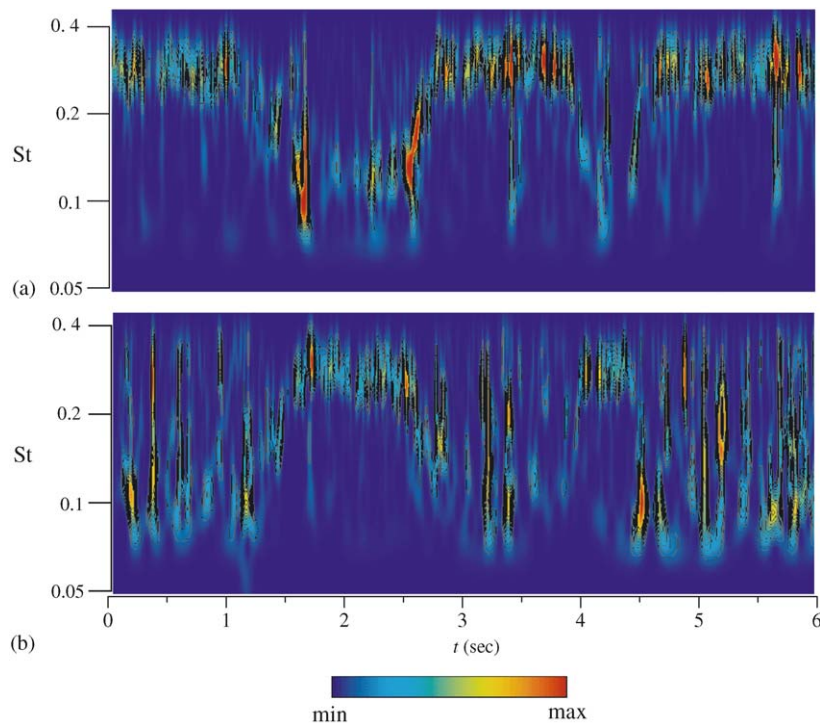Fig. 18. Visualized flow pattern for $T/D = 0.70$: (a) biased flow pattern, (b) nonbiased flow pattern.



Fig. 19. Wavelet power spectrum: (a) signal 1 (hot-wire 1), (b) signal 2 (hot-wire 2). The outer contour line encloses 65% of maximum energy.

where $\omega_0$ is the wave number in the Morlet wavelet, here taken to be 6.0 to satisfy the admissibility condition (Farge, 1992). For $\omega_0 = 6.0$, the relation between scales, $s$, and Fourier frequencies is $f = 1/(1.03\, s)$. The scale was varied in two base logarithms (suggested by Farge, 1992), and the scales had been over sampled by choosing 16 subscales within each scale (Torrence and Compo, 1998).

Wavelet power spectra of two signals obtained simultaneously from the two hot-wires are shown in Fig. 19. Signals 1 and 2 are associated with wake characteristics of cylinders 1 and 2, respectively. Here the spacing between the cylinders was 0.70. The wavelet power spectra show that when the frequency of signal 1 switches from a high-frequency mode of a Strouhal number of 0.28 to a low-frequency mode of a Strouhal number of 0.125, the frequency of signal 2 switches from a low-frequency mode to a high-frequency mode and vice versa. Also, when major switching occurs, both signals possess an intermediate-frequency mode.

The existence of an intermediate frequency stimulated our curiosity to examine what happens in the case of two square-sectioned ($42 \times 42$ mm) cylinders in a side-by-side arrangement. Strouhal number measurements and typical Fourier power spectra are shown in Fig. 20. The Reynolds number in this case was $4.7 \times 10^4$. Three modes of frequency appear in the range of $T/H = 0.40 - 1.9$ also in the case of the two square cylinders. Surprisingly, in the case of two square cylinders, the intermediate-frequency appears for a longer time and sometimes the peak at the intermediate frequency even dominates the peaks at the low and the high frequencies as shown in Figs. 20(b) and (c). A longer appearance of the intermediate frequency can be seen in the wavelet power spectra shown in Fig. 21. The signals whose wavelet power spectra are shown were obtained simultaneously from two hot-wires. The positions of the hot-wires were $1.5 \times H$ outside and $3 \times H$ downstream from the centers of the cylinders. The figure shows that signals 1 and 2 are initially in a high-frequency mode and a low-frequency mode, respectively, then switch to an intermediate-frequency mode at $t = 0.57$ s and then to low- and high-frequency modes at $t = 2$ s. Therefore, it seems that synchronized frequency appears in the range of time of 0.7–1.9 s. Cross-wavelet analysis can be used to trace out the synchronized frequency, synchronized region in time space, and phase relation between the signals.

For two given time series, signals 1 and 2, with wavelet transforms $W_1(s, b)$ and $W_2(s, b)$, the cross-wavelet spectrum can be defined as follows:

$$W_{12}(s, b) = W_1(s, b) W_2^*(s, b), \tag{4}$$

where $W_2^*(s, b)$ is the complex conjugate of $W_2(s, b)$. If the analysis is carried out by means of a complex wavelet, as the Morlet wavelet used in our study, the cross-wavelet spectrum $W_{12}(s, b)$ is also complex, and hence $W_{12}(s, b)$ has real and
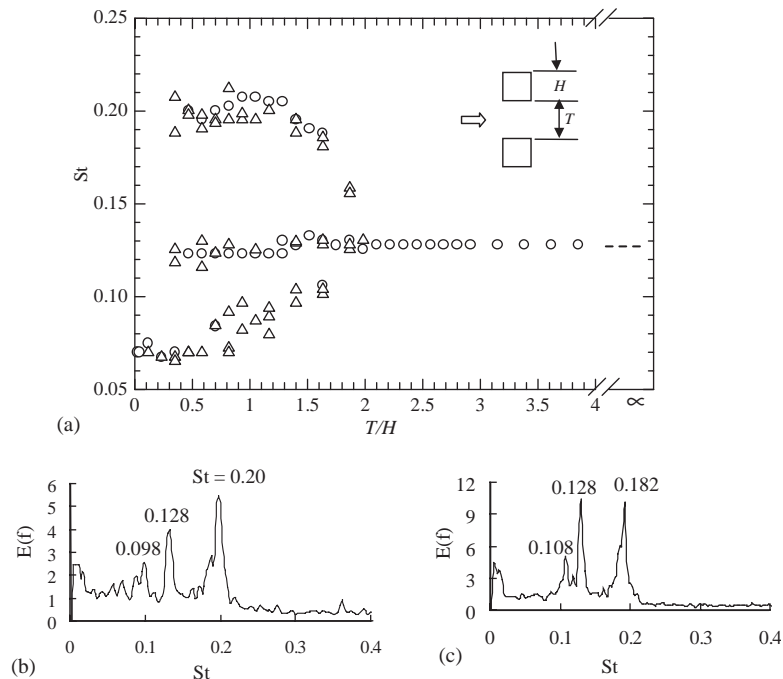


Fig. 20. (a) Strouhal number distribution (square cylinders): $\bigcirc$, fluctuating lift; $\triangle$, hot-wires; - - - - single cylinder; (b) power spectrum of fluctuating velocity, $T/H = 0.90$; (c) power spectrum of fluctuating velocity, $T/H = 1.70$.
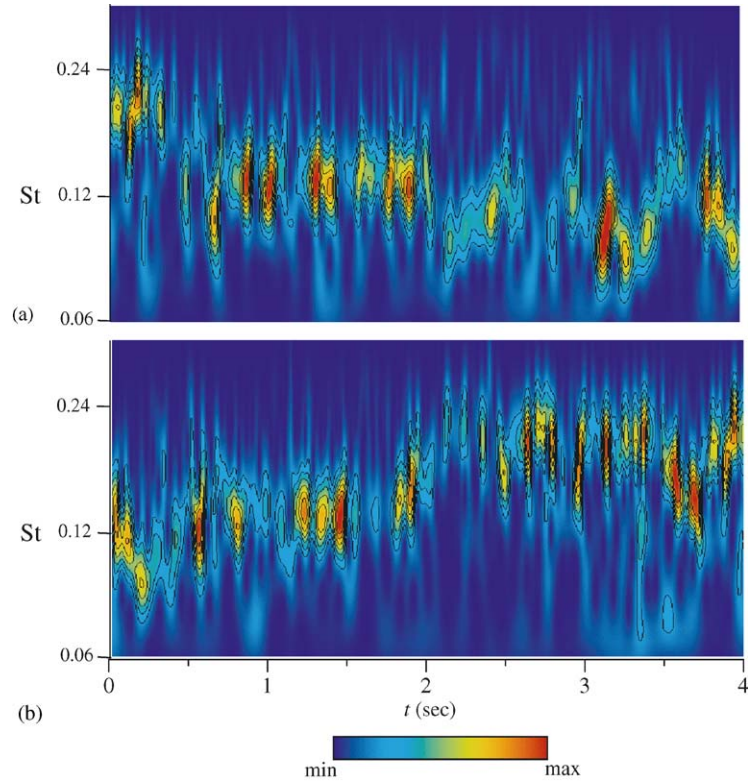
Fig. 21. Wavelet power spectrum for $T/H = 1.2$: (a) signal 1 (hot-wire 1); (b) signal 2 (hot-wire 2). The outer contour line encloses 60% of maximum energy.
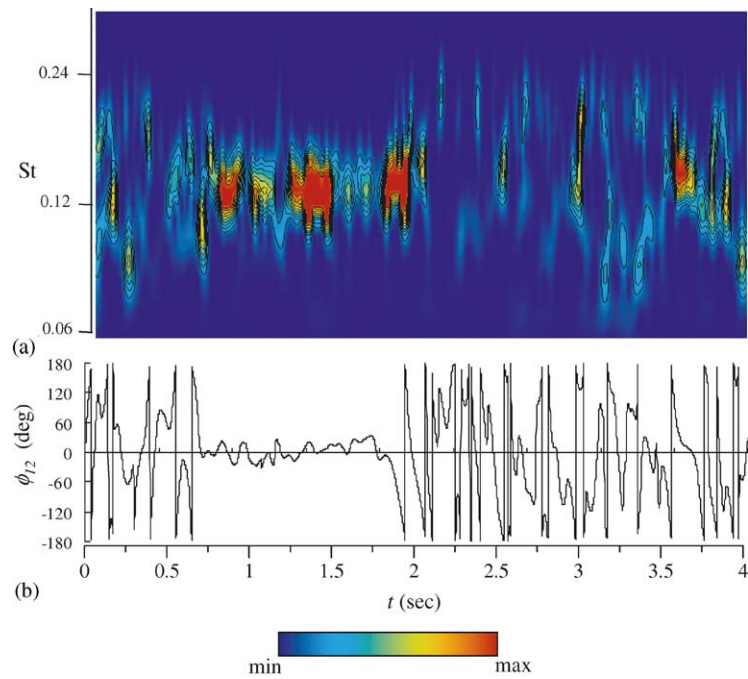


Fig. 22. (a) Cross-wavelet spectrum of signals 1 and 2, and (b) instantaneous phase angle, $\phi_{12}$, between signals 1 and 2 at the Strouhal number of 0.128 (scale $s = 0.0185$).

imaginary parts, $W_{12}^R(s,b)$ and $W_{12}^I(s,b)$, respectively. The magnitude of the cross-wavelet transform $|W_{12}(s,b)|$ indicates the similarity (coherence) between the signals in terms of both frequency and localization (in time space). On the other hand, the instantaneous phase angle between signals 1 and 2 at the scale $s$ can be obtained as

$$\phi_{12}(s,b) = \tan^{-1} \frac{W_{12}^I(s,b)}{W_{12}^R(s,b)}. \tag{5}$$

Fig. 22 shows a cross-wavelet spectrum (Eq. (4)) of the wavelet power spectra presented in Fig. 20. From the figure, we see that the area in which energy is concentrated is at a Strouhal number of 0.128 in the time range 0.7–1.9 s and in the neighborhood of 3.6 s. This implies that the two signals have the same frequency in those time ranges. Fig. 22(b) shows the instantaneous phase angle (Eq. (5)) between the signals at a Strouhal number of 0.128 ($s = 0.0187$). It is interesting that signals 1 and 2 are within $\pm 20°$ of being a $0°$ phase angle in the range of 0.7–1.9 s. This implies that, in the intermediate-frequency mode, the cylinders are shedding vortices in-phase from their outer surfaces; it is known as the antiphase mode (Fig. 2(b)). As will be discussed later in the range of $T/H = 1.9-2.5$, the flow over the cylinders is mainly in an antiphase mode. Thus, the antiphase mode does not suddenly disappear for $T/H < 1.9$; indeed, it appears intermittently for $T/H < 1.9$, causing the appearance of intermediate frequency. The regular modulation of $\phi_{12}$ from $-180°$ to $180°$ indicates that frequencies in signals 1 and 2 in those time spaces are different.

## 3.5. Phase relation

It has been shown that the frequency of vortex shedding of both cylinders is synchronized for $T/D > 1.2$ in the case of circular cylinders and for $T/H > 1.9$ in the case of square cylinders. In the case of synchronized vortex shedding, a predominance of an antiphase mode was observed in flow visualization tests at low Reynolds numbers by Kamemoto (1976), Williamson (1985), Sumner et al. (1999), and Meneghini et al. (2001). Fig. 23 shows a comparative appearances (in a fraction of total time) of antiphase and in-phase modes at various spacings in a wind tunnel test at the Reynolds number of $5.5 \times 10^4$. Instantaneous antiphase and in-phase modes were identified from the local cross-correlation coefficient of fluctuating pressures at the middle of the outer surfaces ($\theta = 90°$) of the cylinders. Therefore, summation of antiphase time, $t_{an}$, and summation of in-phase time, $t_{in}$, in a certain long time, $T_t$, (about 6500 cycles) were obtained and presented as fractions of total time as $\sum t_{an}/T_t$ and $\sum t_{in}/T_t$. The remainder of the total time $T_t - \sum t_{an} - \sum t_{in}$ was neither antiphase nor in-phase. It can be seen in the figure that at just after the threshold spacing (1.2 for circular cylinders and 1.9 for square cylinders) where the three modes of frequency merge and the synchronized frequency starts to appear, the flow profoundly sheds in the antiphase mode: 60% of total time for circular cylinders and 68% for square cylinders. As the spacing increases, the appearance of the antiphase mode decreases and that of the in-phase mode increases. That is, the wake behind the cylinders losses their dependency to shed antiphase mode with an increase of spacing. This result is in good agreement with that of Kamemoto (1976). At $T/D = 1.5$, Kamemoto estimated 40% of time for the antiphase mode and 6% for the in-phase mode. Bearman and Wadcock (1973) estimated cross-correlation coefficients of hot-wire signals at the two outer $90°$ points, and they showed that the correlation coefficient was maximum at $T/D = 1.3$ and that the value of the correlation coefficient decreased with increase in $T/D$. This indicates a predominance of antiphase vortex shedding, and its dominancy decreases with an increase in spacing. At a lower subcritical Reynolds number of $5.8 \times 10^3$ and for $T/D = 1$, Zhou et al. (2002) found an antiphase flow to be dominant by 91% even at $10D$ downstream from the cylinders. A predominance of the antiphase mode was observed in the range of $T/D = 1-2$ and intermittent appearance of antiphase and in-phase modes was observed in the range of $T/D > 2$ also in the flow visualization test. Flow visualization of near wake flow shows the antiphase vortex shedding for $T/D = 1.3$ (Fig. 24(a)) and intermittent antiphase and in-phase vortex shedding for $T/D = 2.4$ (Figs. 24(b) and (c)). Thus, it may be inferred that the predominance of antiphase vortex shedding is independent of the Reynolds number.

## 4. Conclusions

In this study, the characteristics of wake frequency, the switching phenomenon, and fluid forces acting on two circular cylinders in a side-by-side arrangement were investigated in detail. There was a marked bistable nature of the flow in the range of $T/D = 0.10-1.5$. Steady and fluctuating fluid forces induced by a narrower wake (mode 'NW') and a wider wake (mode 'WW') were decomposed from digitally stored data. However, the mode 'NW' caused a higher drag and lower lift forces, while the mode 'WW' caused lower drag and higher lift forces on the respective cylinders. The fluctuating fluid forces ($C_{Df}$ and $C_{Lf}$) were comparatively higher for the 'NW' mode, and the differences in $C_{Df}$ and $C_{Lf}$ induced by modes 'NW' and 'WW' were greater in the range of $T/D = 0.80 \sim 1.20$. For $T/D = 0.10-0.20$ and 1.2–1.50,
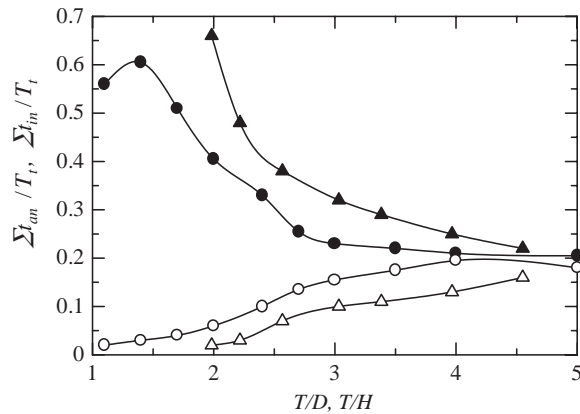
Fig. 23. Antiphase and in-phase patterns at various spacings: ●, antiphase (circular cylinders); ○, in-phase (circular cylinders); ▲, antiphase (square cylinders); △, in-phase (square cylinders).
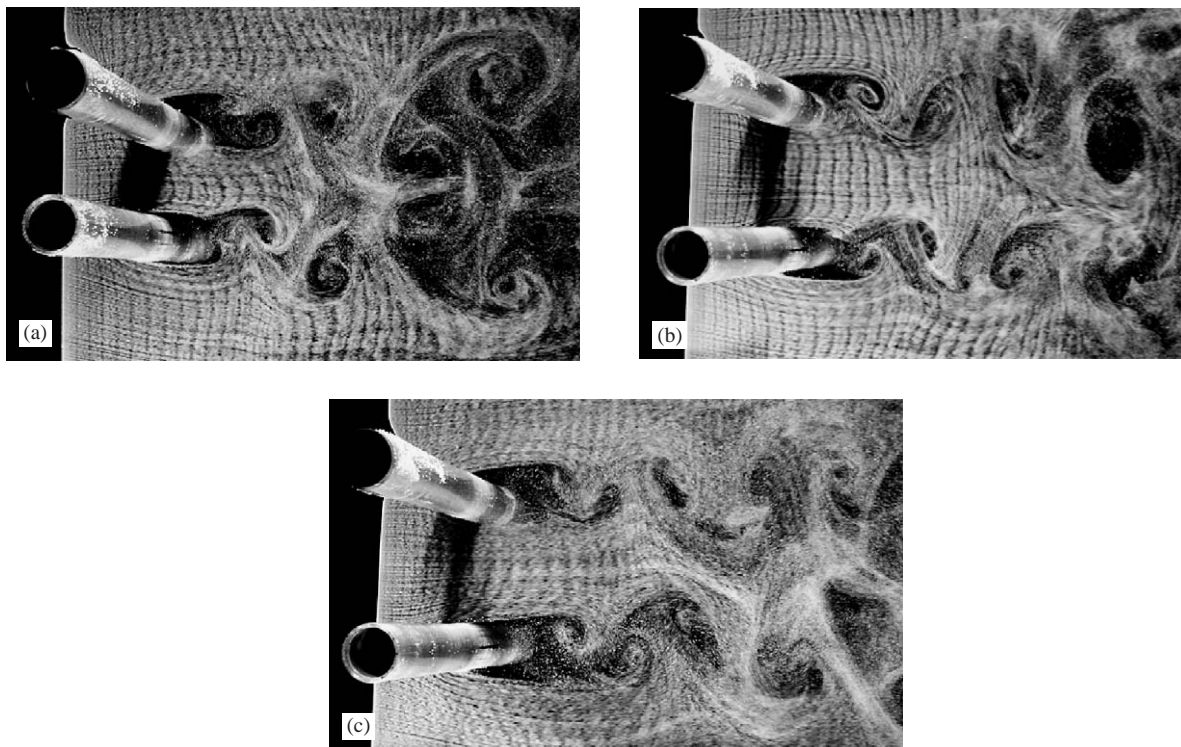


Fig. 24. Flow patterns: (a) antiphase ($T/D = 1.3$), (b) antiphase ($T/D = 2.4$), and (c) in-phase ($T/D = 2.4$).

the mean value of $C_D$ induced by modes 'NW' and 'WW' was greater than that of a single cylinder; these results are different from those obtained by Zdravkovich and Pridden (1977) but agree with those obtained by Hori (1959).

The action of the lift forces on the cylinders was outward (repulsive) for $T/D > 0.20$. However, for $T/D = 0.10$, an inward lift force, $C_L = -0.12$, acted on one cylinder that was associated with mode 'NW' and an outward lift force, $C_L = 0.65$ acted on the other cylinder. At this spacing, there was a large difference in $C_L$ induced by modes 'NW' and 'WW'.

On the basis of frequency, fluid forces, and flow characteristics, the following four distinct regimes of flow were found. (i) At $T/D = 0.10$, the gap flow was highly biased and the two cylinders had the same frequencies. (ii) At

$T/D = 0.20-1.2$, the biased gap flow formed a narrower wake and a wider wake, resulting in a lower frequency in the wider wake and a higher frequency in the narrower wake. When the gap flow switched from one side to the other, there was another intermediate flow of short duration in which the gap flow was oriented parallel to the free-stream flow and the Strouhal number in this mode was almost the same as that found in a single cylinder or for $T/D > 1.2$. This flow pattern was further corroborated by the results of modal analysis and wavelet analysis. (iii) At $T/D = 1.2-1.5$, the gap flow was slightly biased, but there was synchronized antiphase vortex shedding. Wider and narrower wakes induced different fluid forces on the respective cylinders. (iv) At $T/D > 1.5$, both cylinders experienced the same time-averaged drag and fluctuating drag and lift forces. The wakes behind the cylinders were almost independent, though the antiphase vortex was found to be predominant.

Wavelet analysis is a very useful tool for analyzing the switching phenomenon in two side-by-side cylinders. High frequency, intermediate frequency, and low frequency in the signals obtained from hot-wires were detected in wavelet power spectra. Cross-wavelet analysis between two signals is useful to trace out synchronized frequency, the synchronized region in time space, and phase characteristics between the signals.

### References

Alam, M.M., Morya, M., Takai, M., Sakamoto, H., 2003. Fluctuating fluid forces acting on two circular cylinders in a tandem arrangement at a subcritical Reynolds number. Journal of Wind Engineering and Industrial Aerodynamics 91, 139–154.

Arneodo, A., Gresseau, G., Holschneider, M., 1988. Wavelet transform of multifractals. Physics Review Letters 61, 2281–2284.

Batham, J.P., 1973. Pressure distribution on circular cylinders at critical Reynolds numbers. Journal of Fluid Mechanics 57, 209–228.

Bearman, P.W., 1969. On vortex shedding from a circular cylinder in the critical Reynolds number regime. Journal of Fluid Mechanics 37, 577–585.

Bearman, P.W., Wadcock, A.J., 1973. The interaction between a pair of circular cylinders normal to a stream. Journal of Fluid Mechanics 61, 499–511.

Farge, M., 1992. Wavelet transforms and their applications to turbulence. Annual Review of Fluid Mechanics 24, 395–457.

Farrant, T., Tan, M., Price, W.G., 2000. A cell boundary element method applied to laminar vortex-shedding from arrays of cylinders in various arrangements. Journal of Fluids and Structures 14, 375–402.

Guillaume, D.W., LaRue, J.C., 1999. Investigation of the flopping regime with two-, three- and four-cylinder arrays. Experiments in Fluids 27, 145–156.

Hamdan, M.N., Jubran, B.A., Shabaneh, N.H., Abu-Samak, M., 1996. Comparison of various basic wavelets for the analysis of flow-induced vibration of a cylinder in cross-flow. Journal of Fluids and Structures 10, 633–651.

Hori, E., 1959. Experiments on flow around a pair of parallel circular cylinders. Proceedings of 9th Japan National Congress for Applied Mechanics 3, 231.

Jendrzejczyk, J.A., Chen, S.S., 1982. Fluid forces on two circular cylinders in liquid cross-flow. In Flow-Induced Vibration of Circular Cylindrical Structures, ASME PVP 63, pp. 31–44.

Jendrzejczyk, J.A., Chen, S.S., 1986. Fluid forces on two circular cylinders in crossflow. In Flow-Induced Vibration 1986, ASME PVP 104, pp. 1–13.

Kamemoto, K., 1976. Formation and interaction of two parallel vortex streets. Bulletin of the Japan Society of Mechanical Engineers 19, 283–290.

Keefe, R.T., 1961. An investigation of the fluctuating forces acting on a stationary circular cylinder in a subsonic stream and of the associated sound field. University of Toronto, UTIAS Report 76, Toronto, Canada.

Kim, H.J., Durbin, P.A., 1988. Investigation of the flow between a pair of circular cylinders in the flopping regime. Journal of Fluid Mechanics 196, 431–448.

Kiya, M., Arie, M., Tamura, H., Mori, H., 1980. Vortex shedding from two circular cylinders in staggered arrangement. Journal of Fluids Engineering 102, 166–173.

Kolar, V., Lyn, D.A., Rodi, W., 1997. Ensemble-averaged measurements in the turbulent near wake of two side-by-side square cylinders. Journal of Fluid Mechanics 346, 201–237.

Landweber, L., 1942. Flow about a pair of adjacent, parallel cylinders normal to a stream, theoretical analysis. The David Taylor Model Basin, Report 485, pp. 1–27.

Lesage, F., Gartshore, I.S., 1987. A method of reducing drag and fluctuating side force on bluff bodies. Journal of Wind Engineering and Industrial Aerodynamics 25, 229–245.

Lewalle, J., 1994. Wavelet analysis of experimental data: some methods and the underlying physics. AIAA Journal 94, 2281–2288.

Liu, Y., So, R.M.C., Lau, Y.L., Zhou, Y., 2001. Numerical studies of two side-by-side elastic cylinders in a cross-flow. Journal of Fluids and Structures. 15, 1009–1030.

Mahir, N., Rockwell, D., 1996. Vortex formation from a forced system of two cylinders, Part II: side-by-side arrangement. Journal of Fluids and Structures 10, 491–500.

Meneghini, J.R., Satara, F., Siqueira, C.L.R., Ferrari, J.A., 2001. Numerical simulation of flow interference between two circular cylinders in tandem and side-by-side arrangements. Journal of Fluids and Structures 15, 327–350.

Mizushima, J., Takemoto, Y., 1996. Stability of flow past a rows of square bars. Journal of the Physical Society of Japan 65, 1673–1685.

Nebres, J., Batill, S., 1993. Flow about a circular cylinder with a single large-scale surface perturbation. Experiments in Fluids 15, 369–379.

Peschard, I., Gal, P.L., 1996. Coupled wakes of cylinders. Physical Review Letters 77, 3122–3125.

Quadflieg, H., 1977. Vortex induced load on the cylinder pair at high Re. Forschung im Ingenieur Wesen 43, 9–18.

Roshko, A., 1954. On the drag and shedding frequency of two-dimensional bluff bodies. National Advisory Committee for Aeronautics, Technical Note, No. 3169, 1–29.

Sakamoto, H., Oiwake, S., 1984. Fluctuating forces on a rectangular prism and a circular cylinder placed vertically in a turbulent boundary layer. Journal of Fluids Engineering 106, 160–166.

Sakamoto, H., Haniu, H., Obata, Y., Matubara, S., 1994. Optimum suppression of fluid forces acting on a circular cylinder and its effectiveness. JSME International Journal, Series B 37, 369–376.

Slaouti, A., Stansby, P.K., 1992. Flow around two circular cylinders by random-vortex method. Journal of Fluids and Structures 6, 641–670.

So, R.M.C., Savkar, S.D., 1981. Buffeting forces on rigid circular cylinders in crossflow. Journal of Fluid Mechanics 105, 397–425.

Spivack, H.M., 1946. Vortex frequency and flow pattern in the wake of two parallel cylinders at varied spacing normal to an air stream. Journal of the Aeronautical Sciences 13, 289–301.

Sumner, D., Wong, S.S.T., Price, S.J., Paidoussis, M.P., 1999. Fluid behavior of side-by-side circular cylinders in steady cross-flow. Journal of Fluids and Structures 13, 309–339.

Szepessy, S., Bearman, P.W., 1992. Aspect ratio and end plate effects on vortex shedding from a circular cylinder. Journal of Fluid Mechanics 234, 191–217.

Thomas, O.G., Kraus, K.A., 1964. Interaction of vortex streets. Journal of Applied Physics 365, 3458–3459.

Torrence, C., Compo, G., 1998. A practical guide to wavelet analysis. Bulletin of the American Meteorological Society 79, 61–78.

West, G.S., Apelt, C.J., 1982. The effect of tunnel blockage and aspect ratio on the mean flow past a circular cylinder with Reynolds number between $10^4$ and $10^5$. Journal of Fluid Mechanics 114, 361–377.

West, G.S., Apelt, C.J., 1993. Measurements of fluctuating pressures and forces on a circular cylinder in the Reynolds number range $10^4$ to $2.5 \times 10^5$. Journal of Fluids and Structures 7, 227–244.

West, G.S., Apelt, C.J., 1997. Fluctuating lift and drag forces on finite lengths of a circular cylinder in the subcritical Reynolds number range. Journal of Fluids and Structures 11, 135–158.

Williamson, C.H.K., 1985. Evolution of a single wake behind a pair of bluff bodies. Journal of Fluid Mechanics 159, 1–18.

Williamson, C.H.K., 1996. Three dimensional wake transition. Journal of Fluid Mechanics 328, 345–407.

Zdravkovich, M.M., 1977. Review of flow interference between two circular cylinders in various arrangements. Journal of Fluids Engineering 199, 618–633.

Zdravkovich, M.M., Pridden, D.L., 1977. Interference between two circular cylinders: series of unexpected discontinuities. Journal of Industrial Aerodynamics 2, 255–270.

Zhang, H.J., Zhou, Y., 2001. Effect of unequal cylinder spacing on vortex streets behind three side-by-side cylinders. Physics of Fluids 13, 3675–3686.

Zhou, Y., Wang, Z.J., So, R.M.C., Xu, S.J., Jin, W., 2001. Free vibrations of two side-by-side cylinders in a cross-flow. Journal of Fluid Mechanics 443, 197–229.

Zhou, Y., Zhang, H.J., Yiu, M.W., 2002. The turbulent wake of two side-by-side circular cylinders. Journal of Fluid Mechanics 458, 303–332.